JOURNAL OF COMPUTATIONAL PHYSICS **126,** 343–355 (1996)
ARTICLE NO. 0142

Numerical Study for the Three-Dimensional Rayleigh–Taylor Instability through the TVD/AC Scheme and Parallel Computation

X. L. LI,* B. X. JIN,† AND J. GLIMM‡

*Department of Mathematical Science, Indiana University-Purdue University at Indianapolis, Indianapolis, Indiana 46202; †Computing Center, Academia Sinica, China; and ‡Department of Applied Mathematics and Statistics, University at Stony Brook, Stony Brook, New York 11794

Received April 20, 1995; revised January 9, 1996

The Rayleigh–Taylor instability is a gravity driven instability of a contact surface between fluids of different densities. The growth of this instability is sensitive to numerical or physical mass diffusion. For this reason, high resolution of the contact discontinuity is particularly important. In this paper, we address this problem using a second-order TVD finite difference scheme with artificial compression. We describe our numerical simulations of the 3D Rayleigh–Taylor instability using this scheme. The numerical solutions are compared to (a) the exact 2D solution in the linear regime and (b) numerical solutions using the TVD scheme and the front tracking method. The computational program is used to study the evolution of a single bubble and 3D bubble merger, i.e., the nonlinear evolution of a single mode and the process of nonlinear mode–mode interaction.

1. INTRODUCTION

Rayleigh–Taylor instability has attracted the attention of physicists because of its important role in inertially confined nuclear fusion. In the initial state of the Rayleigh–Taylor instability, an interface separates two fluids of different densities. Gravity points from the heavy fluid to the light fluid across an interface which, in the unperturbed configuration, is flat. Such a configuration is unstable. When a small perturbation is introduced, the heavy fluid will fall into the light fluid as a spike and the light fluid will rise into the heavy fluid as a bubble. The single mode bubble motion reaches a steady state motion with constant velocity in a tube or with periodic boundary conditions. A randomly perturbed initial fluid interface produces bubbles of different sizes. Bubbles with large radii advance faster than those with small radii. Merger occurs when a larger bubble bypasses adjacent smaller ones. The envelope of the bubble front is accelerated as a result of this bubble competition.

There are three regimes of Rayleigh–Taylor instability. The first regime occurs when the amplitude of a perturbation is much smaller than the wavelength. In this case, the fluid motion can be analyzed by linear theory; a small perturbation of the fluid interface has an exponential growth

$$h(t) = h_0 e^{\nu t}, \tag{1.1}$$

whre h is the amplitude at time t, h_0 is the initial amplitude, and ν is the growth rate of the perturbation. The growth rate is a function of the density ratio, viscosity, surface tension, and boundary conditions [2].

As a second regime, the unstable mode becomes nonlinear. It grows into bubbles of light fluid and spikes of heavy fluid. The bubble motion in this regime was analyzed by Taylor who gave the scaling law

$$V_B = C\sqrt{AgR} \tag{1.2}$$

for the single mode saturated bubble velocity, where g is the gravity and R is the bubble radius. The Atwood number is $A = (\rho_1 - \rho_2)/(\rho_1 + \rho_2)$, where ρ_1 and ρ_2 are densities of the heavy fluid and the light fluid, respectively. The constant C has been studied experimentally by Taylor [21] and analytically by Garabedian [4]. The commonly accepted values of C for incompressible fluids are 0.32 for a 2D bubble and 0.48 for a 3D bubble.

The interaction among bubbles of different sizes defines the third flow regime and results in competition, merger, and chaotic mixing. The bubble front envelope is accelerated in this regime. Youngs and Read [20, 25] find from experiment that the accelerated motion can be expressed by the formula

$$h = \alpha g A t^2, \tag{1.3}$$

where h is the height of the bubble envelope and t is time. The coefficient α, according to Youngs, is a constant, independent of A. The experimentally measured value of α is about 0.06 for incompressible flow.

Recently, scientists have attempted to simulate chaotic

0021-9991/96 $18.00

mixing through direct numerical solution of the Euler equations in both 2D and 3D. Youngs [26, 27] used a finite difference method to solve both 2D and 3D Euler equations. In his simulation, it is found that the acceleration rate α is about 0.04, which is more than 30% smaller than the value measured in experiment. However, 2D simulations using the front tracking method [10, 8] give close agreement with experiment. Tryggvason also reported good agreement with experiment using his front tracking code for incompressible fluids [22].

Youngs used a second-order TVD van Leer scheme. The front tracking method uses the MUSCL schemes. But in the front tracking method, finite difference numerical solvers are applied to different fluid components separately and the solution at the fluid interface is obtained through the solution of a Riemann problem in the normal direction for each front point. Therefore, numerical diffusion of the fluid density across the density discontinuity has been eliminated in the latter method.

Compared to Youngs' simulation using a TVD van Leer scheme, it is understandable that the front tracking method gives higher resolution to the solution at the fluid interface where the density is discontinuous. However, such a method is more difficult to implement, especially in 3D. In this paper, we introduce a new method which is a compromise between the two methods. The new method is based on a modified TVD scheme with the addition of artificial compression to the linearly degenerate equation for mass conservation. This method significantly improves the resolution at the contact discontinuity. Although this method is not as highly resolved as the front tracking method, its implementation is much simpler.

We compare numerical solutions using the front tracking (FT) method, the TVD scheme, and the TVD scheme with artificial compression (TVD/AC) for two test problems for which the answers are known. We compare solutions in the linear regime of the Rayleigh–Taylor instability and for a single bubble in its terminal velocity regime. We also show TVD/AC solutions for the multi-mode chaotic mixing regime.

2. THE MATHEMATICAL MODEL

The Rayleigh–Taylor instability can be described by the Euler equations for compressible fluids:

$$\frac{\partial \rho}{\partial t} + \nabla \cdot (\rho \mathbf{v}) = 0 \tag{2.1}$$

$$\frac{\partial \mathbf{v}}{\partial t} + (\mathbf{v} \cdot \nabla)\mathbf{v} = -\frac{\nabla p}{\rho} + \mathbf{g} \tag{2.2}$$

$$\frac{\partial (\rho E)}{\partial t} + \nabla \cdot (\rho \mathbf{v}(E + P)) = \rho \mathbf{v} \cdot \mathbf{g} \tag{2.3}$$

In 3D, the equations can be written in the conservation form

$$q_t + F^1_x + F^2_y + F^3_z = H \tag{2.4}$$

where q is a vector, and F^1, F^2, F^3 are the flux functions in the x, y, and z directions, respectively, and H is the source vector, namely,

$$q = \begin{pmatrix} \rho \\ \rho E \\ \rho u \\ \rho v \\ \rho w \end{pmatrix}, \quad F^1 = \begin{pmatrix} \rho u \\ \rho u(E+P) \\ \rho u^2 + P \\ \rho uv \\ \rho uw \end{pmatrix}, \quad F^2 = \begin{pmatrix} \rho u \\ \rho v(E+P) \\ \rho vu \\ \rho v^2 + P \\ \rho vw \end{pmatrix}, \tag{2.5}$$

$$F^3 = \begin{pmatrix} \rho w \\ \rho w(E+P) \\ \rho wu \\ \rho wv \\ \rho w^2 + P \end{pmatrix}, \quad H + \begin{pmatrix} 0 \\ \rho wg \\ 0 \\ 0 \\ \rho g \end{pmatrix}.$$

We solve the above equations numerically, by a method based on Mulder, Osher, and Sethian [16] for simulation in 2D and extended to 3D by Li [14]. The numerical method includes a second-order finite difference solver, the level set method [18] to trace and reconstruct the fluid interface, and a parallelization algorithm. The major difference between this paper and the previous paper [14] lies in the application of a high resolution finite difference scheme for the contact discontinuity. We mention other interface enhancing algorithms, such as SLIC [23]; detailed comparisons are outside of the scope of the present paper.

In the previous paper [14], we used a second-order TVD scheme [19]. This scheme is effective for solving problems of shock wave propagation. In it, physical compression compensates for the numerical diffusion across a shock front. However, numerical diffusion still exists when the characteristics associated with a discontinuous wave do not converge into it in a shock-line fashion. The contact discontinuity in the Rayleigh–Taylor instability is not compressive in this sense. Therefore, if the TVD scheme is applied to such a problem, the fluid interface is diffusive. The initially sharp front becomes smeared-out over an increasingly wider diffusion zone as time increases. In this paper, we emphasize that the width of the smeared contact discontinuity governs the overall accuracy of such computations as the Rayleigh–Taylor instability and is thus a significant figure of merit for these computations. From this point of view, we conclude that the front tracking method is most desirable for such problems but is more

difficult to implement in three dimensions due to its complexity. The TVD/AC implementation in 3D is a compromise between the previous work using the level set method and the front tracking method. For the Rayleigh–Taylor instability problem, it is a very efficient method with enhanced resolution and accuracy.

The mass diffusion of the contact discontinuity is an important factor which affects the accuracy of the numerical solution of the Rayleigh–Taylor instability. The importance of mass diffusion can be demonstrated by both Youngs' experimental results and the numerical solution using resolution-enhancing mechanisms. Youngs reported his experimental results of the Rayleigh–Taylor instability with more than two layers of fluids. When a layer of fluid with an intermediate density is applied, Youngs found that the acceleration is reduced through the empirical formula:

$$h = 0.06(Agt^2 - \eta\Delta), \tag{2.6}$$

where Δ is the width of the intermediate layer and η, according to Youngs, is a constant. To show the effect of the intermediate layer, we used the 2D front tracking method. The results show that when an intermediate layer is introduced in the Rayleigh–Taylor instability, the terminal velocity of the single bubble is substantially reduced. Figure 1 presents a comparison of fluid interfaces in simulations with and without intermediate layers.

The new numerical scheme by Jin [13] is based on the original TVD scheme and the pioneering work of Harten [12]. This method pays special attention to the contact discontinuity in the numerical simulation. In order to maintain the sharp boundary of the contact wave, we follow Harten and Yang [24] and introduce artificial compression in the TVD scheme. In this way, the linearly degenerate equation of mass conservation behaves as a compressive wave such as a shock wave in the TVD scheme. The details of this scheme are given in Section 3. We show that TVD/AC gives much higher resolution than TVD to the interface in the numerical solution of Rayleigh–Taylor instability. More importantly, the 2–3 block numerical diffusion in TVD/AC does not spread further as time increases. This behavior is in sharp contrast to TVD, for which the mass diffusion zone grows wider with increasing time. TVD/AC thus offers significant improvements over TVD for the solution of the Rayleigh–Taylor instability. The level set method for interface tracing is a postprocessing step and has no role (other than postcomputation graphical analysis) in the computations presented here, but it could be used to resolve equation of state issues in mixed material cells for multi-material. Rayleigh–Taylor simulations.

As with other numerical methods, TVD/AC with the level set method has its shortcomings and limitations. It uses about 80% more CPU time than the TVD scheme to compute the artificial compression. The lack of active tracking of the fluid interface introduces an error in the computation when the equations of state of the two fluids are different. The discussion of this problem and the successful implementation of the 3D front tracking method have been given in the paper by Glimm *et al.* [7]. For problems such as the shock-contact interaction, the front tracking method tends to give better and more accurate solutions [11].

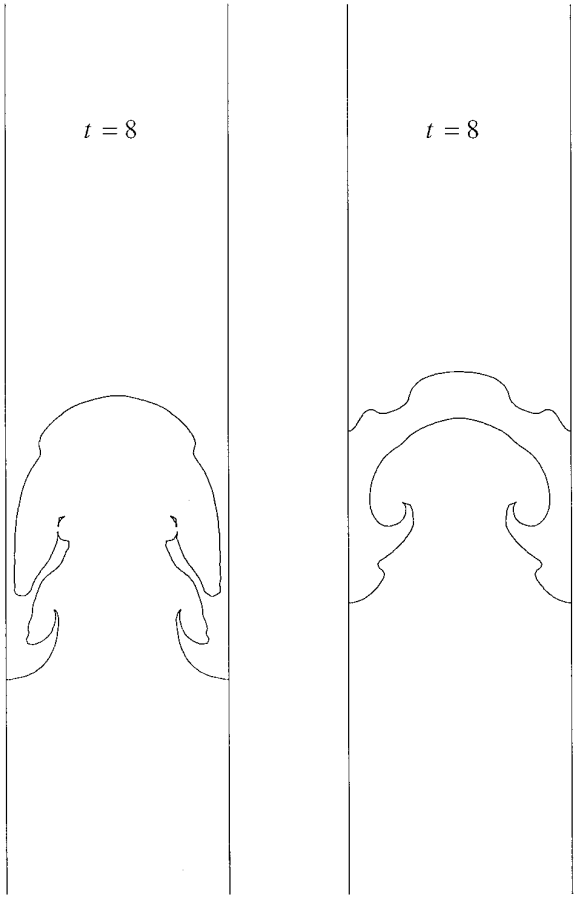

FIG. 1. Interface plots of 2D simulations using the front tracking method. The left is a two layer simulation and the right is a simulation with three layers. On the right, a layer with intermediate fluid density is placed in the middle while all other physical parameters are unchanged. The initial width of the intermediate layer is about eight computational mesh blocks. The numerical simulation shows a significantly slower evolution of the bubble, here located at the outside edges of the computational strip, and moving downward.

3. TVD SCHEME WITH ARTIFICIAL COMPRESSION

3.1. *Scalar Equations*

Schemes such as TVD and ENO (essentially non-oscillatory) for the finite difference solution of conservation laws have enhanced the resolution of shock waves. However,

these schemes are not well suited for the study of fluid contact discontinuities. Using these schemes, numerical solutions are increasingly smeared out across a contact interface as time advances.

The contact discontinuity occurs in a linearly degenerate wave equation. Consider the following scalar linear wave equation

$$\frac{\partial u}{\partial t} + a\frac{\partial u}{\partial x} = 0. \tag{3.1.1}$$

The TVD scheme advances the solution via the equation

$$u_j^{n+1} = u_j^n - \lambda(f_{j+1/2}^n - f_{j-1/2}^n), \tag{3.1.2}$$

where $f_{j+1/2}^n$ is the numerically calculated flux

$$f_{j+1/2}^n = \tfrac{1}{2}(au_j^n + au_{j+1}^n + g_j^n + g_{j+1}^n - Q(a + \lambda_{j+1/2}^n)\Delta_{j+1/2}^n), \tag{3.1.3}$$

$$g_j^n = M(\tilde{g}_{j-1/2}^n, \tilde{g}_{j+1/2}^n), \tag{3.1.4}$$

$$\tilde{g}_{j+1/2}^n = \tfrac{1}{2}(Q(a) - \lambda a^2)\Delta_{j+1/2}^n, \tag{3.1.5}$$

$$\Delta_{j+1/2}^n = u_{j+1}^n - u_j^n, \tag{3.1.6}$$

and M is the minmod function,

$$M(x_1, x_2, ..., x_n) = \begin{cases} \operatorname{sign}(x_1)\min(|x_1|, |x_2|, ..., |x_n|), & \text{all } x_i \text{ have same sign} \\ 0, & \text{otherwise.} \end{cases} \tag{3.1.7}$$

Here we have assumed $Q(x) = |x|$, $\lambda = \Delta t/\Delta x$, and

$$\gamma_{j+1/2}^n = \begin{cases} (g_{j+1}^n - g_j^n)/\Delta_{j+1/2}^n, & \Delta_{j+1/2}^n \neq 0, \\ 0, & \Delta_{j+1/2} = 0. \end{cases} \tag{3.1.8}$$

The flux term $f_{1+1/2}^n$ can be written as the flux in the Lax–Wendroff scheme plus a viscous term, that is,

$$f_{1+1/2} = f_{j+1/2}^{\mathrm{LW}} + V_{\mathrm{isc}}, \tag{3.1.9}$$

where $f_{j+1/2}^{\mathrm{LW}} = (a/2)\,(u_j^n + u_{j+1}^n) - \frac{1}{2}\lambda a^2\Delta_{j+1/2}^n$ is the flux in a Lax–Wendroff scheme. Also, with V_{isc} given by (3.1.9), we define $\mu_{j+1/2}$ through the formula

$$V_{\mathrm{isc}} = -\mu_{j+1/2}\Delta_{j+1/2}^n. \tag{3.1.10}$$

From this definition, we observe that $\mu_{j+1/2}$ satisfies

$$0 \le \mu_{j+1/2} \le \tfrac{1}{2}|a|(1 - \lambda|a|)(1 - r_{j+1/2}), \tag{3.1.11}$$

where

$$r_{j+1/2} = M\left(1, \frac{\Delta_{j-1/2}}{\Delta_{j+1/2}}, \frac{\Delta_{j+3/2}}{\Delta_{j+1/2}}\right). \tag{3.1.12}$$

Thus $0 \le r_{j+1/2} \le 1$. V_{isc} is a viscous term and dissipates numerical oscillations. In the case of a shock wave, since the characteristic field is compressive, the existence of V_{isc} will not make the transition region grow with increasing time. However, in the linear case, the characteristic field is no longer compressive, and V_{isc} causes the mass diffusion region to increase with time. It will therefore seriously decrease the resolution of the numerical solution. To enhance the resolution, one must compensate for the effect of V_{isc}. Artificial compression provides such a compensation.

Harten [12] originated the idea of artificial compression. Yang [24] combined artificial compression and ENO. He demonstrated that artificial compression effectively reduces numerical diffusion across a contact discontinuity. This idea was extended by Jin to the TVD scheme which we use in this paper. Jin's method is easy to implement and is also effective in reducing numerical diffusion across a contact discontinuity. Artificial compression has no effect on compressive waves. In smooth regions, the numerical scheme maintains second-order accuracy.

In the scalar case, in order to eliminate the effect of the V_{isc} term, we need to apply Eqs. (3.1.2)–(3.1.5) to (3.1.1):

$$\frac{\partial u}{\partial t} + \frac{\partial}{\partial x}(au + \mathrm{L}(u)) = 0, \tag{3.1.13}$$

where $L(u)$ is an anti-diffusion term to cancel the V_{isc}. Equation (3.1.13) is a modified form of Eqs. (3.1.2)–(3.1.5). From this we have a new numerical flux

$$f_{j+1/2}^n = \tfrac{1}{2}(au_j^n + au_{j+1}^n + L^n + L_{j+1}^n + g_j^n + g_{j+1}^n - Q(a + v_{j+1/2}^{LM} + \gamma_{j+1/2}^n)\Delta_{j+1/2}^n), \tag{3.1.14}$$

where

$$v_{j+1/2}^{LM} = \begin{cases} (L_{j+1}^n - L_j^n)/\Delta_{j+1/2}^n, & \Delta_{j+1/2}^n \neq 0, \\ 0, & \Delta_{j+1/2}^n = 0, \end{cases} \tag{3.1.15}$$

and the definition of $\gamma_{j+1/2}^n$ is the same as Eq. (3.1.8),

$$\tilde{g}_{j+1/2} = \tfrac{1}{2}(Q(a + v_{j+1/2}^{LM}) - \lambda(a + v_{j+1/2}^{LM})^2)\,\Delta_{j+1/2}^n. \tag{3.1.16}$$

To preserve all properties of the TVD scheme, we take L_j^n to be the form

$$L_j^n = S \cdot \max(0, M(\eta L_{j-1/2}^n, L_{j+1/2}^n) \cdot S, M(L_{j-1/2}^n, \eta L_{j+1/2}^n) \cdot S). \tag{3.1.17}$$

Here $S = \text{sign}(L_{j+1/2}^n)$ and

$$L_{j+1/2}^n = \tfrac{1}{2}(Q(a) - \lambda a^2)(\Delta_{j+1/2}^n - M(\Delta_{j-1/2}^n, \Delta_{j+1/2}^n, \Delta_{j+3/2}^n)). \tag{3.1.18}$$

The purpose of η is to keep L_j^n to be of $O(\Delta x^2)$ in an interval for which the solution is smooth, and to be $O(1)$ in an interval of discontinuity. We take η to have the form

$$\eta = 2\left|\frac{|\Delta_{j+1/2}^n|^\beta - |\Delta_{j-1/2}^n|^\beta}{|\Delta_{j+1/2}^n|^\beta + |\Delta_{j-1/2}^n|^\beta}\right|, \quad \beta = 2.5. \tag{3.1.19}$$

When $\eta \approx 0$ (this occurs when $|\Delta_{j-1/2}^n| \approx |\Delta_{j+1/2}^n|$), the scheme is the same as the TVD scheme. In this way, we avoid making a smooth solution into a discontinuous one. It can be proved that the new scheme does not change the order of accuracy of the TVD scheme. On the other hand, at the hill and cliff regions of discontinuity where the difference between $|\Delta_{j-1/2}^n|$ and $|\Delta_{j+1/2}^n|$ is large, the effect of finite η (therefore finite L_j^n) will contribute to the flux like a source term. The extent to which η affects the steepening of the discontinuity can be adjusted by changing the value of β.

3.2. *One-Dimensional Systems of Equations*

The 1D Euler equations have the form

$$\frac{\partial q}{\partial t} + \frac{\partial f(q)}{\partial x} = 0, \tag{3.2.1}$$

where $q = (\rho, \rho u, \rho E)$, $f(q) = (\rho u, p + \rho u^2, u(p + \rho E))$, and ρ, u, p, E denote density, velocity, pressure, and specific energy

$$E = \frac{u^2}{2} + \frac{1}{\gamma - 1}\frac{p}{\rho},$$

with γ the gas constant.

The system has three characteristics corresponding to eigenvalues $a^1 = u - c$, $a^2 = u$, and $a^3 = u + c$, where c is the speed of sound. The second characteristic is linearly degenerate. Using Roe averages, we determine $a_{j+1/2}^i$ and the corresponding eigenvectors $R_{j+1/2}^i$, $i = 1, 2, 3$. Applying artificial compression to the linearly degenerate characteristics, we obtain the finite difference scheme

$$q_j^{n+1} = q_j^n - \lambda(f_{j+1/2}^n - f_{j-1/2}^n), \tag{3.2.2}$$

$$f_{j+1/2} = \frac{1}{2}\left(f_j^n + f_{j+1}^n + \sum_{k=1}^{3} \phi_{j+1/2}^k \cdot R_{j+1/2}^k\right), \tag{3.2.3}$$

$$\phi_{j+1/2}^k = g_j^k + g_{j+1}^k - Q(a_{j+1/2}^k + \gamma_{j+1/2}^k)d_{j+1/2}^k, \quad k = 1, 2, 3, \tag{3.2.4}$$

where $d_{j+1/2}^k$ satisfy

$$q_{j+1}^n - g_j^n = \sum_{k=1}^{3} d_{j+1/2}^k \cdot R_{j+1/2}^k \tag{3.2.5}$$

$$g_j^k = M(\tilde{g}_{j-1/2}^k, \tilde{g}_{j+1/2}^k), \quad k = 1, 3, \tag{3.2.6}$$

$$g_j^2 = M(\tilde{g}_{j-1/2}^k, \tilde{g}_{j+1/2}^2) + L_j \tag{3.2.7}$$

$$\tilde{g}_{j+1/2}^k = \tfrac{1}{2}(Q(a_{j+1/2}^k) - \lambda(a_{j+1/2}^k)^2)\, d_{j+1/2}^k, \quad k = 1, 2, 3, \tag{3.2.8}$$

$$\gamma_{j+1/2}^k = \begin{cases} (g_{j+1}^k - g_j^k)/d_{j+1/2}^k, & d_{j+1/2}^k = 0, \\ 0, & d_{j+1/2}^k \neq 0, \end{cases} \tag{3.2.9}$$

$$Q(x) = \begin{cases} |x|, & |x| > \varepsilon \\ \dfrac{1}{2\varepsilon}(x^2 + \varepsilon^2), & |x| \le \varepsilon, \end{cases} \tag{3.2.10}$$

and ε is a positive constant generally taken to be between 0.1 to 0.5. Also

$$L_j = S \cdot \max(0, S \cdot M(\eta L_{j-1/2}, L_{j+1/2}), S \cdot M(L_{j-1/2}, \eta L_{j+1/2})), \tag{3.2.11}$$

$S = \text{sign}(L_{j+1/2})$,

$$L_{j+1/2} = \tfrac{1}{2}(Q(a_{j+1/2}^2) - \lambda(a_{j+1/2}^2)^2)(d_{j+1/2}^2 - M(d_{j-1/2}^2, d_{j+1/2}^2, d_{j+3/2}^2)), \tag{3.2.12}$$

$$\eta = 2\left|\frac{|d_{j+1/2}^2|^\beta - |d_{j-1/2}^2|^\beta}{|d_{j+1/2}^2|^\beta + |d_{j-1/2}^2|^\beta}\right|, \quad \beta = 2.5. \tag{3.2.13}$$

3.3. *Three-Dimensional Split Implementation*

In 3D, Eq. (2.5) is solved through a TVD scheme with the addition of artificial compression to the linearly degenerate equations. The numerical scheme can be implemented as

$$q^* = g^n + \Delta t L(q^n), \quad q^{n+1} = g^n + \tfrac{1}{2}\Delta t(L(q^n) + L(q^*)), \tag{3.3.1}$$

where $L(q^n) = L^1(q^n) + L^2(q^n) + L^3(q^n) + H(q^n)$. The functions L^l, $l = 1, 2, 3$, are the difference operators for

the flux in the three coordinate directions. They are the second-order TVD scheme with artificial compression. At the node point (x_i, y_j, z_k), the difference operator in the x-direction can be written

$$[L^1(q^n)]_{ijk} = h^1_{i+1/2,jk} - h^1_{i-1/2,jk}. \tag{3.3.2}$$

If $\{R^m\}_{m=1}^5$ are the eigenvectors of the Jacobi matrix and $\partial F^1/\partial q$ and $\{a^m\}_{m=1}^5$ are the corresponding eigenvalues, then

$$h^1_{i+1/2,jk} = \tfrac{1}{2}\,(F^1_{i,jk} + F^1_{i+1,jk} - \sum_{m=1}^{5} s^m_{i+1/2,jk} R^m_{i+1/2,jk}) \tag{3.3.3}$$

where

$$(R^1, R^2, R^3, R^4, R^5) = \begin{pmatrix} 1 & 1 & 1 & 0 & 0 \\ H - uc & K & H + uc & -v & -w \\ u - c & u & u + c & 0 & 0 \\ v & v & v & -1 & 0 \\ w & w & w & 0 & -1 \end{pmatrix}, \tag{3.3.4}$$

$H = E + P/\rho$ is the enthalpy, $K = \frac{1}{2}(u^2 + v^2 + w^2)$ is proportional to the kinetic energy, and $c = \sqrt{\gamma(P/\rho)}$ is the sound speed. The eigenvalues of this matrix are

$$(a^1, a^2, a^3, a^4, a^5) = (u - c, u, u + c, u, u). \tag{3.3.5}$$

$$\begin{aligned} s^m_{i+1/2,jk} = {} & g^m_{i,jk} + g^m_{i+1,jk} + C^m_{i,jk} + C^m_{i+1,jk} \\ & - |a^m_{i+1/2,jk} + \nu^m_{i+1/2,jk} + \mu^m_{i+1/2,jk}| d^m_{i+1/2,jk} \end{aligned} \tag{3.3.6}$$

$\{\mathrm{d}^m_{i+1/2,jk}\}_{m=1}^5$ satisfy

$$q_{i+1,jk} - q_{i,jk} = \sum_{m=1}^{5} d^m_{i+1/2,jk} R^m_{i+1/2,jk}, \tag{3.3.7}$$

where the values at $x_{i+1/2,jk}$ are given by Roe's average [11], i.e.,

$$q_{i+1/2,jk} = \frac{\sqrt{\rho_{i,jk}}\, q_{i,jk} + \sqrt{\rho_{i+1,jk}}\, q_{i+1,jk}}{\sqrt{\rho_{i,jk}} + \sqrt{\rho_{i+1,jk}}} \tag{3.3.8}$$

and

$$g^m_{i,jk} = \mathrm{mind}(g^m_{i-1/2,jk}, g^m_{i+1/2,jk}), \tag{3.3.9}$$

where the function mind is defined as $\mathrm{mind}(a, b) = \mathrm{sign}(a) \max\{0, \min\{\mathrm{sign}(b)a, |b|\}\}$, and

$$\begin{aligned} g^m_{i+1/2,jk} = {} & \tfrac{1}{2}\,|a^m_{i+1/2,jk} + \mu^m_{i+1/2,jk}|\,[1 - \lambda|a^m_{i+1/2,jk} \\ & + \mu^m_{i+1/2,jk}|]\, d^m_{i+1/2,jk}. \end{aligned} \tag{3.3.10}$$

The term $C^m_{i,jk}$ is the artificial compression. It can be written

$$\begin{aligned} C^m_{i,jk} = {} & \mathrm{sign}(C^m_{i+1/2,jk}) \max\{\mathrm{mind}(\eta C^m_{i-1/2,jk}, C^m_{i+1/2,jk}), \\ & \mathrm{mind}(C^m_{i-1/2,jk}, \eta C^m_{i+1/2,jk})\}, \end{aligned} \tag{3.3.11}$$

where

$$\begin{aligned} C^m_{i+1/2,jk} = {} & \tfrac{1}{2}\,|a^m_{i+1/2,jk}|[1 - \lambda|a^m_{i+1/2,jk}|][d^m_{i+1/2,jk} \\ & - \mathrm{mind}(d^m_{i-1/2,jk}, d^m_{i+1/2,jk}, d^m_{i+3/2,jk})] \end{aligned} \tag{3.3.12}$$

(see [12] for further detail), and

$$\mu^m_{i+1/2,jk} = \frac{C^m_{i+1,jk} - C^m_{i,jk}}{d^m_{i+1/2,jk}}, \quad \nu^m_{i+1/2,jk} = \frac{g^m_{i+1,jk} - g^m_{i,jk}}{d^m_{i+1/2,jk}}. \tag{3.3.13}$$

Similarly, we can obtain the difference operators in the y and z directions.

4. THE NUMERICAL RESOLUTION OF CONTACT DISCONTINUITIES

We compare numerical Riemann solutions using the TVD and TVD/AC schemes.

4.1. *Comparison of* 1D *Numerical Solutions*

We first consider the scalar equation $u_t + au_x = 0$. The initial condition for u has a jump from 0 to 1. We define N_d to be the total number of mesh blocks lying between the solution contours $u = 0.1$ and $u = 0.9$. For the TVD scheme, the numerical simulation shows that N_d increases with time. At the 500th time step, N_d has reached the value 11 (see Fig. 2a, case $\beta = 0.0$), while for the TVD/AC solution with $\beta = 2.5$, N_d grows to a constant value, here equal to 1.94, for the entire computation. We want to emphasize that the front tracking method maintains $N_d = 0$ in the computation. Figure 2b shows the comparison of the numerical solutions at a fixed time step.

Similar comparisons were performed for systems of equations. Figure 3 compares TVD and TVD/AC Riemann solutions for gas dynamics. The graphs show density vs distance at time step 50. The width of the contact discontinuity in the TVD scheme is about 7–8 mesh blocks while it is only about 3–4 blocks for TVD/AC. We should mention that while artificial compression is important in sharpening the contact discontinuity, it also has the tendency to steepen the rarefaction wave, particularly while the rarefaction is very steep, at the beginning of its spreading-

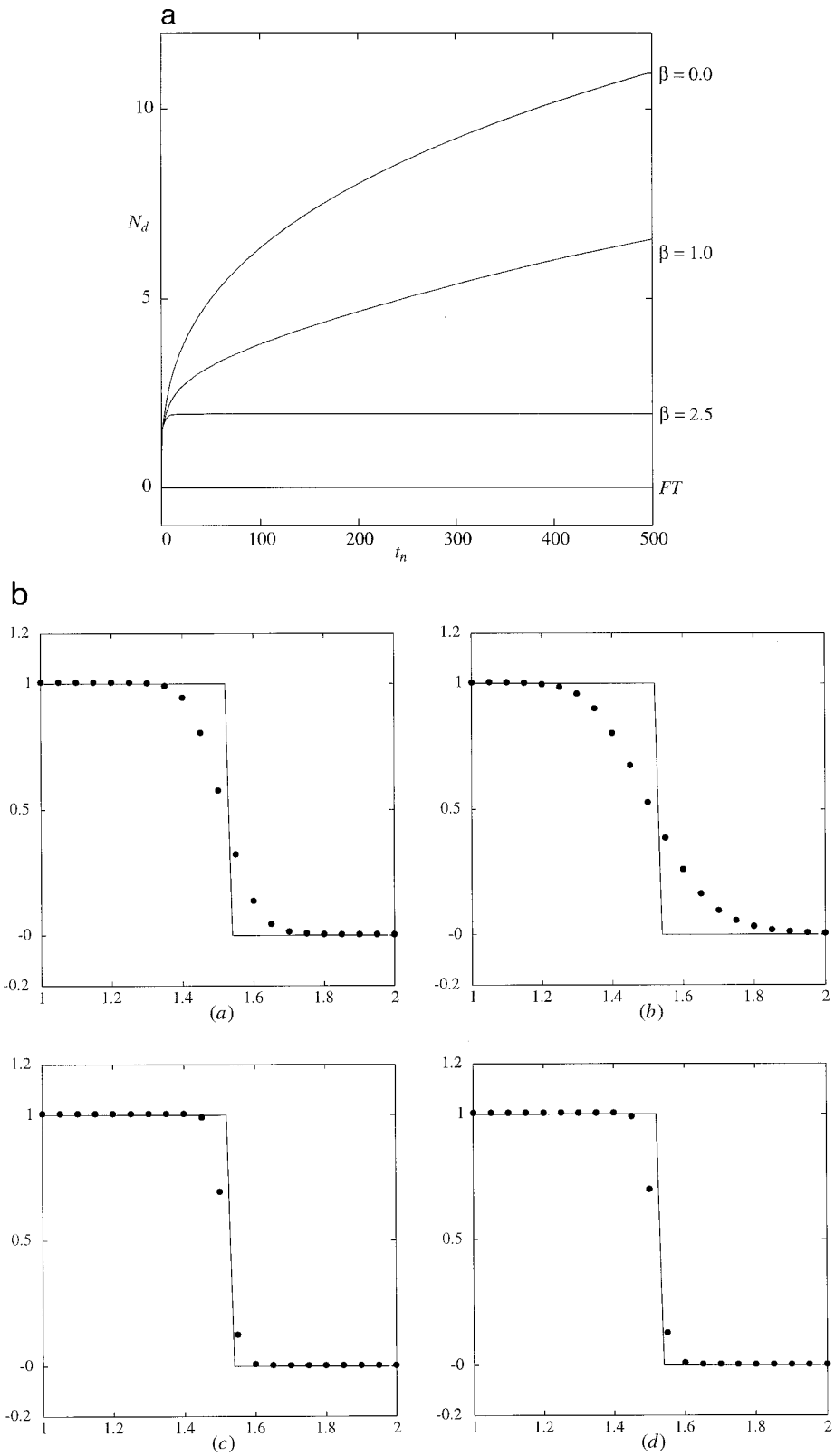

FIG. 2. a. The width of numerically smeared-out contact discontinuity (N_d) vs time step (t_n). This quantity is derived from the numerical solution to the scalar equation $u_t + au_x = 0$ using the TVD scheme with varying artificial compression parameter β. The width is defined as the number of mesh blocks between $u = 0.1$ and $u = 0.9$. The FT case is from the front tracking method. b. Comparison of numerical solutions using the TVD scheme and the TVD/AC scheme. These are solutions of the equation $u_t + au_x = 0$. The graphs are u vs $x - at$. Figures 2a and 2b at the top give comparison of the TVD solutions with the exact solutions at time steps 50 and 400, respectively. Figures 2c and 2d are solutions from the TVD/AC scheme at the same time steps 50 and 400, respectively.

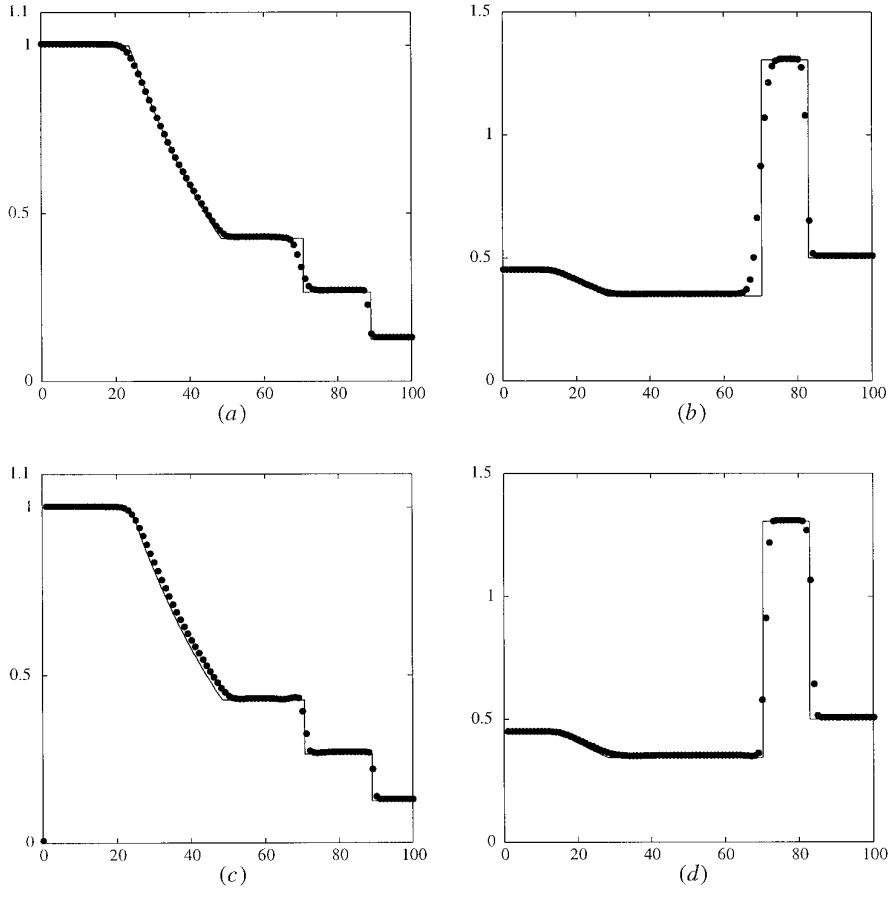

FIG. 3. Comparison of numerical solutions using the TVD scheme and the TVD/AC scheme. The upper two graphs diaplay the numerical solutions of the TVD scheme and the lower two graphs display solutions of the TVD/AC scheme. The left two graphs present the solutions of the Riemann problem with $(p_L, d_L, u_L) = (1, 1, 0)$ and $(p_R, d_R, u_R) = (0.1, 0.125, 0)$. While the right two graphs present solutions of the Riemann problem with $(p_L, d_L, u_L) = (3.538, 0.445, 0.698)$ and $(p_R, d_R, u_R) = (0.571, 0.5, 0)$.

out. But its effect on the rarefaction is less serious after the rarefaction has already spread out. At such time, the change of gradient in density profile is much smaller than that at the contact discontinuity. This can be seen by comparing the rarefaction part of Riemann solution in Fig. 3a and Fig. 3c. Figure 3c shows that artificial compression does not affect the overall accuracy of the rarefaction wave.

4.2. *The 2D Growth Rate of the Rayleigh–Taylor Instability*

We compare the TVD/AC, TVD and front tracking schemes for the linear growth rate of a small amplitude single mode Rayleigh–Taylor instability in two dimensions. In these simulations, the front tracking method maintains a sharp contact discontinuity with no numerical diffusion across the interface, TVD/AC maintains a steady mass diffusion zone of 2–3 mesh blocks for the density gradient, while TVD has a relatively large and growing diffusion zone.

The width of the density discontinuity affects the growth rates of the Rayleigh–Taylor instability in the linear regime. Table I shows the comparison of the growth rate of the unstable interface using the three methods. In this set of experiments, the compressibility is $M^2 = 0.01$ and the Atwood number is 0.818 (density ratio 10 : 1). The exact linear growth rate, 0.846, was calculated through the formulas of [5]. The initial amplitude of the perturbation as a function of wavelength is 0.01. We measured the growth rate between $t = 0.1$ and $t = 0.2$ for all three methods. For a 128×128 computational mesh, the front tracking method gives the highest growth rate and is the closest to the exact solution with only 1.8% relative error. The error in the TVD/AC growth rate is about 3.7% smaller than the exact solution, the TVD error is about 3.8%. The growth rate in TVD/AC is closer to the exact solution than that of TVD when the computational mesh is coarse while the difference narrows as the mesh becomes finer. The growth rate decreases when the amplitude becomes larger

TABLE I

Comparison of Linear Growth Rates for the Rayleigh–Taylor Instability Using Different Numerical Methods

Mesh size	ν_T	ν_A	ν_F	e_T	e_A	e_F
8×8	0.602	0.680	0.754	0.288	0.196	0.109
16×16	0.720	0.741	0.779	0.149	0.124	0.079
32×32	0.756	0.770	0.784	0.106	0.090	0.073
64×64	0.798	0.803	0.814	0.057	0.051	0.038
128×128	0.814	0.815	0.831	0.038	0.037	0.018
256×256	0.834	0.834	0.843	0.014	0.014	0.004

Note. The compressibility in this case is $M^2 = 0.01$ and the Atwood number is $A = 0.82$. The exact linear growth rate is $\nu = 0.846$, ν_T, ν_A, and ν_F are growth rates from the simulations using TVD, TVD/AC, and front tracking methods, respectively. e_T, e_A, and e_F are the relative errors of the three methods $e_{T,A,F} = |(\nu_{T,A,F} - \nu)/\nu|$, respectively.

because of nonlinear effects. The nonlinear solutions themselves were used to determine the time period of validity of the linear (analytic) solution. The measurement of linear growth rate is a sensitive experiment. The values presented in Table I are measured in the time period which we believe to be closest to the linear regime.

5. 3D PARALLEL COMPUTATION OF BUBBLE MOTION

The TVD/AC code is parallelized using a domain decomposition method to divide the volume into cubic subdomains. See also Li [14]. The program has been tested on two parallel environments. One is the Intel-iPSC/860 hypercube computer at SUNY Stony Brook. The other is a cluster of 20 SUN stations connected by the software PVM (parallel virtual machine). The efficiency of the latter is about 50% due to the data communication overhead through ethernet.

5.1. *Simulation of a Single Bubble*

We tested the convergence of a single bubble using the TVD/AC scheme. Figure 4 shows the fluid interface with different levels of mesh refinement. We observe that increased mesh refinement adds more detailed structure to the vortex rollup, but that convergence of the large scale structure, including the bubble and spike fronts, has been achieved. The finer scale structure does not converge, in the sense that new structures appear as the mesh is refined, unless some stabilizing feature, such as surface tension is added [6].

Figure 5 compares the resolution of the light–heavy fluid interface (the spike front) using the TVD/AC scheme with β varying from 0.0 to 3.0. As we can see from the comparison, after 975 time steps, the $\beta = 2.0$–3.0 cases maintain a much sharper density front than that of the $\beta = 0.0$ case

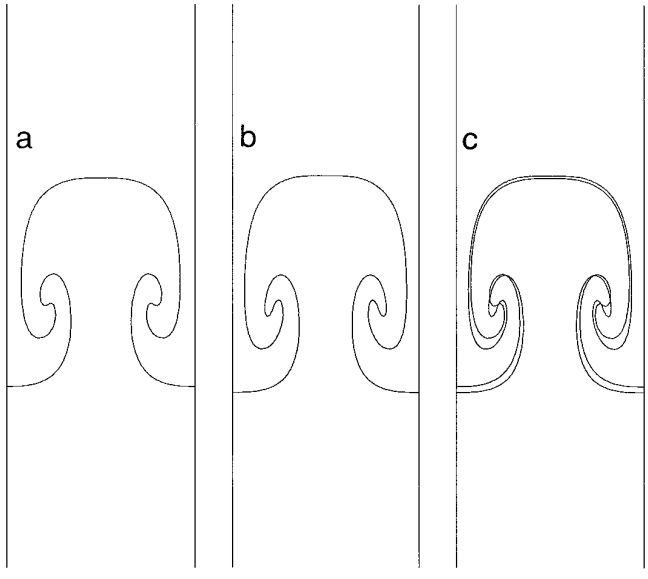

FIG. 4. Convergence test of a 2D single bubble interface with the TVD/AC scheme. Plot (a) is the fluid interface with a 50×150 computational mesh; (b) is the fluid interface with a 100×300 mesh; (c) is the superposition of the two interfaces. The density ratio is 5:3 ($A = 0.25$) and the compressibility is $M^2 = 0.1$.

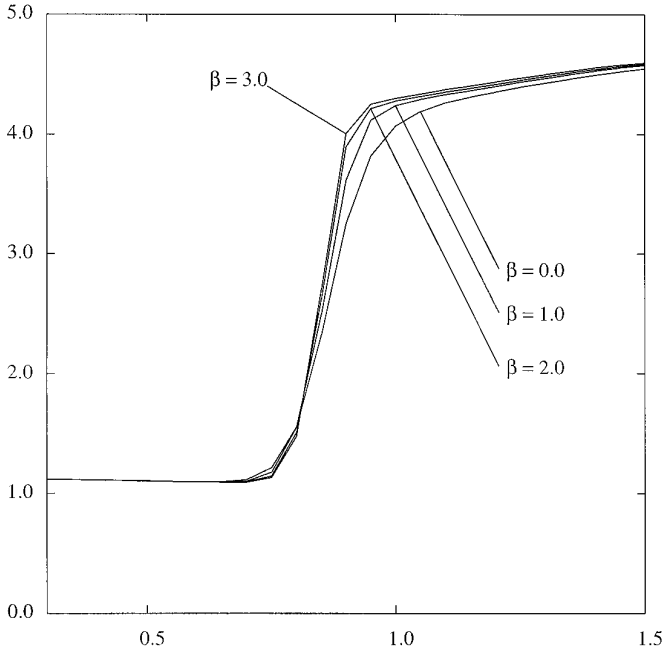

FIG. 5. Comparison of the density profile at the fluid interface (spike front) in the Rayleigh–Taylor instability. The four cases in the figure have different coefficients of artificial compression (β). It is found that when $\beta \geq 2.0$, the steepening of the density profile at the interface is saturated. In most of the physical simulations reported in this paper we chose $\beta = 2.5$.

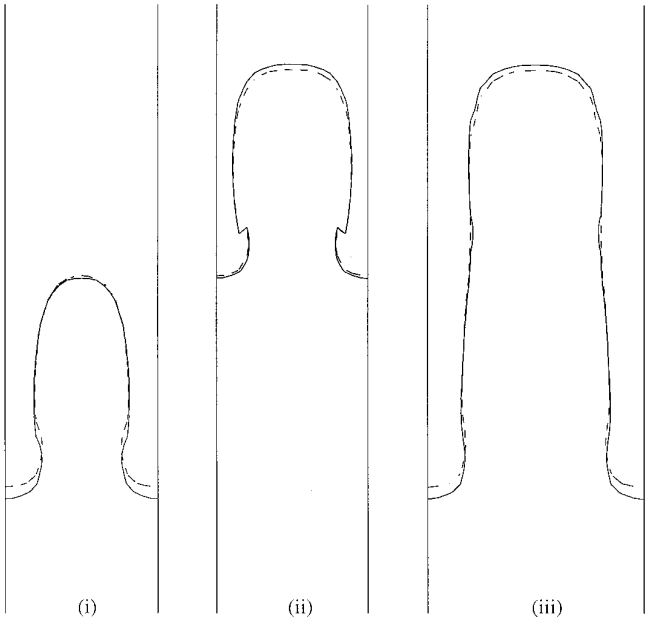

FIG. 6. Comparison of the fluid interfaces in simulations using TVD and TVD/AC schemes, respectively. The plot (i) is the cross section through spike front; (ii) is the cross section through the bubble front; (iii) is the diagonal cross section through both bubble and spike. The simulation is performed on a $20 \times 20 \times 80$ computational mesh. We note the close agreement between these simulations, with the TVD bubble retarded relative to the TVD/AC bubble.

(original TVD). The sharpening of the contact surface becomes saturated when $\beta \geq 2.5$. Therefore, throughout the physical simulation of the Rayleigh–Taylor instability, we choose the value $\beta = 2.5$. Figure 6 is the comparison of the interface for the two methods using the level set description. The computational grid is $20 \times 20 \times 80$, which is relatively coarse. The difference between the solutions by these two methods is decreased by mesh refinement.

We also compare the terminal bubble velocity of the single mode Rayleigh–Taylor instability, as computed by the TVD/AC method. Theoretical and experimental results for the bubble velocity of an incompressible fluid are given by Taylor [21], Birkhoff and Carter [1], and Garabedian [4]. The results show that the final velocity using TVD/AC agrees with these accepted values in the incompressible limit within 14%. It should be mentioned that since we use the rectangular computational domain with periodic boundaries in both x and y directions, the geometric configuration is not identical to that assumed in the analytical model, for which the bubble is axisymmetric. Moreover, the computation is slightly compressible, while the comparison is incompressible.

The simulation of a single bubble was performed for several values of the Atwood number A and a fixed value of compressibility $M^2 = 0.1$, where $M^2 = g\lambda/c_b^2$, λ is the characteristic bubble dimension (diameter), and c_b is the sound speed in the heavy fluid. Table II summarizes the results of the simulation. Figures 7a and 7b show the 3D interface evolution with time. The interface is constructed through the level set function, which traces the motion of the discontinuity in the simulation. Figures 7c shows cross-sectional plots of the interface. Frame (i) displays the front at the bubble cross sections, frame (ii) displays the front at the spike cross sections, and frame (iii) displays cross sections in a diagonal direction, cutting both the bubble and the spike tips. Figure 8, for contrast, shows the effect of an increase at Atwood number and should be compared to Fig. 7b. Note that at this larger Atwood number, there is considerably less roll up at the spike tip, as is to be expected.

5.2. *Simulation of Bubble Merger*

Bubble merger is an important process in the Rayleigh–Taylor instability, leading to the acceleration of the overall fluid interface with a randomly perturbed initial interface [9]. We have used our TVD/AC code to simulate bubble merger. Figure 9 shows the interface in the simulation of a four bubble interaction. We have studied the acceleration of the bubble front under different ratios of bubble radii (the ratio of the largest bubble to the smallest bubble). In a set of experiments with compressibility $M^2 = 0.1$ and Atwood number $A = 0.67$, it is found that when such ratio is about 0.7 : 0.3, the bubble front shows a constant acceleration throughout the merger process. The average acceleration rate α is about 0.05. While not directly comparable to the value $\alpha = 0.06$ measured by Read and Youngs [20, 25], experimentally, for a random interface with incompressible flow, we note that the acceleration observed here is of the expected magnitude.

Glimm *et al.* reported that in the 2D simulation of Ray-

TABLE II

Average BubbleTerminal Velocity in the 3D Simulation of Rayleigh–Taylor Instability Using the TVD/AC Scheme

A	V_b	ΔV_b	C
0.33	0.071	0.008	0.56
0.67	0.089	0.009	0.50
0.82	0.113	0.011	0.55
0.90	0.120	0.008	0.56

Note. The computational mesh in these simulations is $40 \times 40 \times 160$. The computations were performed on 20 SPARC-LX/SPARC-II stations using PVM (parallel virtual machine). The compressibility in these simulations is $M^2 = 0.1$. ΔV_b is the fluctuation in the velocity measurement, due to pressure wave reflections from the boundaries. The agreement with the comparison value of 0.48 within 14% of C is satisfactory in view of the difference in details of the problem formulation from that of the analytic/experimental model and in view of the 10% velocity fluctuation, which limits the precision to which C is determined in this computation.

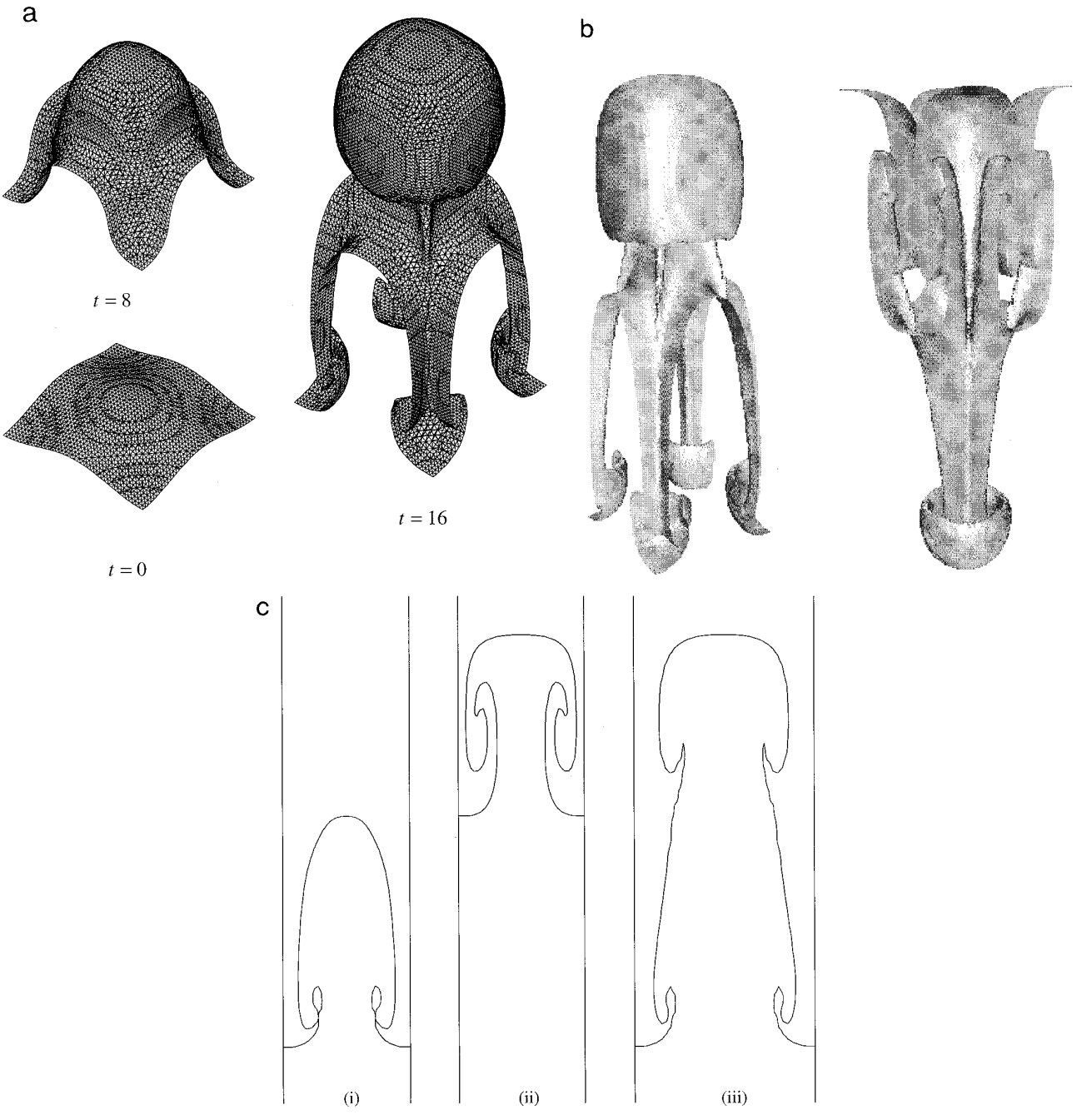

FIG. 7. a. The time evolution of the 3D triangulated interface. The compressibility is $M^2 = 0.1$, and the Atwood number is $A = 0.333$ (density ratio 2:1). The computation uses the TVD/AC scheme with a $40 \times 40 \times 160$ computational mesh. b. Continuation of the 3D interface from Fig. 7a. The left plot is the interface viewed in the bubble periodic section and the right is the same interface offset by a half period, to give the spike periodic section. Interface with lighting reconstructed by using the 3D graphics software Geomview from University of Minnesota. c. Cross-sectional plots of the 3D interface in Fig. 7b ($t = 19$). Plot (i) is the cross section at the spike front; (ii) is the cross section at the bubble front; (iii) is the diagonal cross section through both the bubble and the spike.

leigh–Taylor instability using the front tracking method, the acceleration rate of the bubble envelope increases with compressibility. This trend has been observed in two additional runs with larger compressibility. We have observed that the acceleration does increase but not to the extent reported by Glimm *et al.* The acceleration rate in a run with compressibility $M^2 = 0.2$ is about 0.054. Again the acceleration rates are not directly comparable. Further studies, including mesh refinement and code comparison would be needed to refine this analysis.

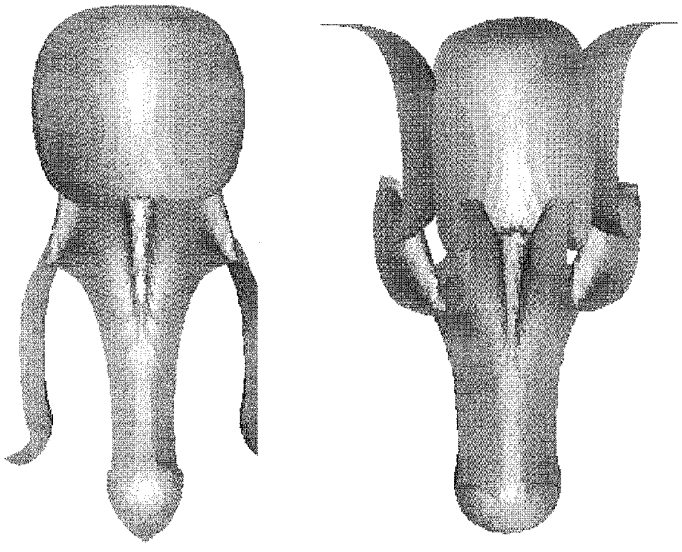

FIG. 8. A 3D interface at late time. The compressibility is $M^2 = 0.1$, and the Atwood number is $A = 0.6$ (density ratio 4 : 1). The computation uses the TVD/AC scheme with a $40 \times 40 \times 160$ computational mesh. The left plot is the interface viewed in the bubble periodic section and the right is the same interface offset by a half period to give the spike periodic section.

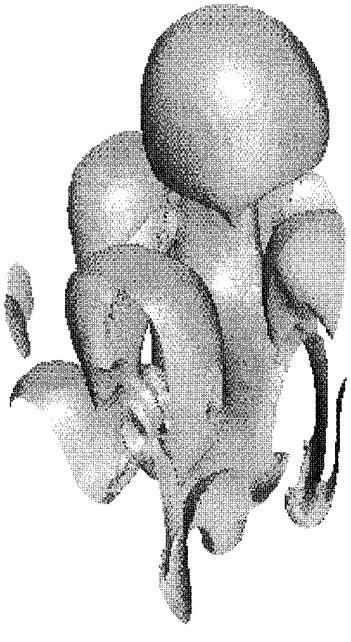

FIG. 9. A 3D interface plot from a bubble merger simulation at $t = 12$. The compressibility is $M^2 = 0.1$, and the Atwood number is $A = 0.667$ (density ratio 5 : 1). The computation uses the TVD/AC scheme with a $40 \times 40 \times 160$ computational mesh. The interface with lighting is reconstructed by using the 3D graphics software Geomview from University of Minnesota. The average acceleration of the bubble front measured during the merger process is $\alpha = 0.05$.

6. DISCUSSION

We have extended the TVD/AC numerical scheme to 3D space. The numerical method is parallelized using the domain decomposition method. We have carried out numerical simulations of single bubble motion and bubble merger, the first of which has been validated by convergence tests under mesh refinement and by comparison to the analytic and experimental values.

The TVD scheme for solving the conservation laws of gas dynamics is diffusive for linearly degenerate waves such as contact discontinuities. Numerical simulations in 2D show that numerical diffusion of the density in the TVD scheme retards the motion of the fluid interface in the Rayleigh–Taylor instability. A new scheme significantly reduces numerical diffusion by adding artificial compression to the TVD scheme. This method confines the numerical diffusion width of the density gradient to 2–3 mesh blocks; moreover, this width does not increase as time advances. The new scheme improves the numerical solution of the Rayleigh–Taylor instability. The 2D comparison among the linear growth rates of the perturbed interface using TVD, TVD/AC, front tracking, and the exact solution shows that the front tracking method, which has a perfectly sharp density gradient, gives a more accurate growth rate, especially for a coarse computational mesh. TVD/AC is better than TVD in the resolution of the contact discontinuity, a fact which is very important in the accurate simulation of the Rayleigh–Taylor instability. On the other hand, compared to the front tracking method, TVD/AC is more efficient to be implemented in three dimensions. It is also much easier to vectorize and parallelize for computation.

ACKNOWLEDGMENTS

This paper is dedicated to Professor B. X. Jin who passed away in July 1994. He had made important contributions to the numerical theory in this paper. J. Glimm and X. L. Li are partially supported by the U.S. Department of Energy, Grant No. DE-FG02-90ER25084.

REFERENCES

1. G. Birkhoff and D. Carter, *J. Math. Mech.* **6,** 769 (1957).
2. S. Chandrasekhar, *Hydrodynamics and Hydromagnetic Stability* (Oxford Univ. Press, Oxford, 1961).
3. I.-L. Chern, J. Glimm, O. McBryan, B. Plohr, and S. Yaniv, *J. Comput. Phys.* **62**(1), 83 (1986).
4. P. R. Garabedian, *Proc. R. Soc. London A* **241,** 81 (1950).
5. C. Gardner, J. Glimm, O. McBryan, R. Menikoff, D. H. Sharp, and Q. Zhang, *Phys. Fluids* **31**(1), 447 (1988).
6. J. Glimm, *SIAM REV.* **33,** 626 (1991).
7. J. Glimm, J. Grove, X. L. Li, K. Shyue, Y. Zeng, and Q. Zhang, *SIAM J. Sci. Comput.*, submitted.
8. J. Glimm, X. L. Li, Q. Zhang, R. Menikoff, and D. H. Sharp, *Advances*

in Compressible Turbulent Mixing (Springer-Verlag, New York/Berlin, 1992), p. 85.

9. J. Glimm and X. L. Li, *Phys. Fluids* **31**(1), 2077 (1988).
10. J. Glimm, X. L. Li, R. Menikoff, D. H. Sharp, and Q. Zhang, *Phys. Fluids A* **2**(1), 2046 (1990).
11. J. Grove, R. Holmes, D. H. Sharp, Y. Yang, and Q. Zhang, *Phys. Rev. Lett.* **71** (21), 3473 (1993).
12. A. Harten, *J. Comput. Phys.* **49,** 357 (1983).
13. B. X. Jin, *Comput. Math.* (*China*) **1,** 121 (1993).
14. X. L. Li, *Phys. Fluids A* **5**(1), 1904 (1993).
15. K. O. Mikaelian, *Phys. Fluids* **6**(1), 356 (1994).
16. W. Mulder, S. Osher, and J. Sethian, *J. Comput. Phys.* **100**(1) 209 (1992).
17. S. A. Orzag and D. Shvarts, ''Simulation and Analysis of 3-D Rayleigh–Taylor and Richtmyer–Meshkov Instabilities, in *4th International Workshop on the Physics of Compressible Turbulent Mixing, March 29–April 1, 1993, Cambridge, UK.*
18. S. Osher and J. Sethian, *J. Comput. Phys.* **79**(1), 12 (1988).
19 S. Osher and S. Chakravarthy, *SIAM J. Numer. Anal.* **21,** 955 (1984).
20. K. I. Read, *Phys. D* **12**(1), 45 (1984).
21. G. I. Taylor, *Proc. R. Soc. London A* **201,** 192 (1950).
22. G. Tryggvason and S. O. Unverdi, *Phys. Fluids A* **2**(1), 656 (1990).
23. W. Noh and P. Woodward, *SLIC* (*Simple Line Interface Calculation*), Lecture Notes in Physics, Vol. 59 (Springer-Verlag, New York, 1976).
24. H. Yang, *J. Comput. Phys.* **89,** 125 (1990).
25. D. L. Youngs, *Phys. D* **37,** 270 (1989).
26. D. L. Youngs, *Phys. D* **12,** 32 (1984).
27. D. L. Youngs, *Phys. Fluids A* **1**(3), 1312 (1991).
28. D. L. Youngs, private communication.
29. N. J. Zabusky, and R. Samtaney, ''Vortex Deposition and Evolution of Perturbed 3-D Richtmyer–Meshkov Instability,'' in *4th International Workshop on the Physics of Compressible Turbulent Mixing, March 29–April 1, 1993, Cambridge, UK.*